Scripta Materialia 284 (2026) 117482

Contents lists available at ScienceDirect

Scripta Materialia

journal homepage: www.journals.elsevier.com/scripta-materialia

# Ultrafast synthesis of Bi–Sr–Ca–Cu–O superconductor within seconds via thermal shock

Vivienne Yiwei Liu [a,1], Weiyin Chen [b,1], Yimeng Huang [b,1], Zihan Lin [a], Ethan Yupeng Zheng [a], Yaoshen Niu [a], Bowen Zhang [b], Ju Li [a,b,*]

[a] Department of Materials Science and Engineering, Massachusetts Institute of Technology, Cambridge, MA, 02139, USA
[b] Department of Nuclear Science and Engineering, Massachusetts Institute of Technology, Cambridge, MA, 02139, USA

ARTICLE INFO

*Keywords:*
Non-equilibrium processing
Ultrafast materials synthesis
Cuprate superconductors
High-temperature superconductivity
Bi–Sr–Ca–Cu–O (Bi–2212)

ABSTRACT

Conventional synthesis of cuprate superconductors typically requires hours to days of thermal processing, hindering rapid exploration of synthesis conditions and materials space. In contrast, ultrafast processing techniques capable of accessing high temperatures on short timescales can significantly accelerate data-driven materials discovery. Here, we demonstrate the formation of a superconducting phase in the Bi–Sr–Ca–Cu–O system by thermal shock within seconds in air. Direct-current (DC) and alternating-current (AC) susceptibility measurements confirm the presence of superconductivity, with a superconducting transition temperature of 90–92 K, consistent with $Bi_2Sr_2CaCu_2O_{8+y}$. Thermal shock is achieved by indirect Joule heating using a pre-oxidized tungsten sheet, enabling ~100 × faster synthesis than conventional solid-state processing. Thermal shock is further extended to the Y–Ba–Cu–O superconductor synthesis. These results establish thermal shock as a promising approach for rapid screening of superconducting oxide chemistries and their appropriate synthesis conditions.

After the discovery of high-temperature oxide superconductors, considerable efforts have been devoted to identifying new superconducting compositions. The lack of a universally accepted microscopic theory for unconventional superconductivity makes rational design challenging. Alternative approaches, such as high-throughput data-driven materials exploration, may provide new insights for oxide superconductor discovery. However, the practical implementation of such an approach is limited by the prolonged synthesis times of oxide superconductors, ranging from hours to days of solid-state reaction for cuprates [1–6], or epitaxial growth followed by topotactic reduction for nickelates [7–9].

There has been a long-standing association between lattice metastability and high-temperature superconductivity [1,10–14]. For example, all known Y–Ba–Cu–O superconductors are metastable at room temperature [10,14]. Only when the synthesis temperature is high enough, such that the entropic contribution can stabilize the geometric misfit, does lower-temperature superconductivity starts to emerge [14,30]. To this end, high-temperature and out-of-equilibrium synthesis methods, capable of accessing metastable phases at high temperatures, followed by fast cooling, are attractive. Existing ultrafast processing techniques, such as carbothermal shock (CTS) [15], ultrafast high-temperature sintering (UTS) [16], and flash Joule heating (FJH) [17], can reach ~$10^3$ K within seconds, followed by a fast cooling rate (~$10^2$ to $10^5$ K $s^{-1}$). These methods have been widely used for the synthesis of multi-element catalysts [15,18], Li-ion battery cathodes [19], and solid-state electrolytes [20]. However, they rely on carbon-based heating elements and therefore require inert atmospheres or vacuum conditions [15–17], which are incompatible with cuprate synthesis. Excess hole doping, thus the presence of oxygen, is essential for superconductivity to emerge in cuprate superconductors [6]. An ultrafast synthesis approach that is suitable for synthesis in air is critical.

Bismuth-based cuprate superconductor, $Bi_2Sr_2CaCu_2O_{8+y}$ (Bi–2212), first reported in 1988, is one of the most studied high-temperature superconducting oxides [21]. Superconducting Bi–Sr–Ca–Cu–O oxide samples are usually synthesized via solid-state reaction at 1073–1143K for 5–24 h under atmospheric conditions, often combined with subsequent repeated grinding and re-sintering or oxygen annealing [3–5,21]. Evidence indicates that the superconducting phase in the Bi–2212 family

* Corresponding author at: Department of Materials Science and Engineering, Massachusetts Institute of Technology, Cambridge, MA, 02139, USA.
*E-mail address:* liju@mit.edu (J. Li).
[1] These authors have contributed equally.

https://doi.org/10.1016/j.scriptamat.2026.117482
Received 28 April 2026; Received in revised form 14 June 2026; Accepted 4 July 2026
Available online 4 July 2026

is stable at elevated temperatures within an appropriate synthesis temperature window due to the entropic contribution to free energy [14]. Short-duration of sintering at elevated temperatures is effective in increasing the relative amount of phases with high superconducting transition temperature ($T_c$, defined from the onset of the diamagnetic response) [4,21]. The observation that a high synthesis temperature corresponds to a high $T_c$ value is not only present in the Bi–Sr–Ca–Cu–O family, but was also seen in other superconducting cuprates [14,22].

In this work, we demonstrate the synthesis of a superconducting phase within the Bi–Sr–Ca–Cu–O system using thermal shock (TS) within seconds in air. The indirect Joule heating is achieved via pre-oxidized tungsten (W) substrate, which operates under ambient conditions and delivers heating and cooling rates of ~ 200 K $s^{-1}$ and ~ 300 K $s^{-1}$, respectively. The resulting superconducting phase exhibits $T_c$ of approximately 90–92 K, exceeding the $T_c$ achieved by single-step solid-state sintering in air.

Fig. 1A shows the TS setup schematic. A cold-pressed Bi–Sr–Ca–Cu–O precursor pellet is subjected to indirect Joule heating delivered by pre-oxidized W substrates mounted on a graphite plate. The graphite plate provides mechanical support and stable electrical contact, while W serves as the resistive heater. To synthesize cuprates in air, a non-carbon substrate simultaneously satisfying three criteria is needed: (i) a high melting temperature to provide a sufficient thermal processing window, (ii) adequate electronic conductivity to drive effective Joule heating, and (iii) low specific heat capacity to realize rapid heating and cooling. Based on these considerations, W foil (W metal with $WO_3$ surface) was selected as the heating substrate; it simultaneously provides high melting temperature (3696 K), moderate electronic conductivity (~4.0 × $10^6$ S/m at 1000 K), and low specific heat capacity (~132 J/(kg·K)). Under ambient conditions, W readily forms $WO_{3-x}$ ($0 \leq x \leq 0.1$) at temperatures as low as 723 K [23]. The formation of $WO_{3-x}$ is exothermic and increases emissivity, leading to a sharp temperature spike on pristine W within the first 5 s of TS due to its radiative heat loss (Fig.S1). To improve heating uniformity, $WO_{3-x}$ layer is pre-formed by passing 40 A through a pristine W strip (0.05 mm × 6 mm × 25 mm) along the length. After approximately 5 s, a visible color change to the pristine W strip surface is observed. The formed oxide layer shows coexisting blue and yellow regions, indicating the formation of $WO_{2.9}$ and $WO_3$ [24] (Fig. 1B). High-resolution X–ray photoelectron spectroscopy (HR–XPS) confirms substantial oxidation of thermal shocked W strip, including the formation of $WO_3$ and other reduced $WO_{3-x}$ species (Fig.S2). In contrast, the pristine W strip shows predominantly metallic W only after 100 s of $Ar^+$ sputtering at 4 keV, indicating that oxidation is much more pronounced after TS (Fig.S3). The use of $WO_{3-x}$ coated W substrate delivers a uniform temperature profile, with only a 10 K rise within ~ 13 s of isothermal hold (Fig. 2A). The preformed $WO_{3-x}$ layer eliminates transient heating non-uniformity associated with W oxidation during TS.

Oxide-based precursor powders $Bi_2O_3$ (99.9%), SrO (99.9%), CaO (99.9%), and CuO (99.99%), purchased from Sigma Aldrich, were used to prepare samples for both TS and solid-state sintering. Oxide-based powders, instead of carbonate-based powders, were chosen to minimize unwanted traces of carbonate phases [5]. Precursors were mixed by mortar and pestle according to the molar ratio of Bi:Sr:Ca:Cu = 2:2:1:2. A pressed green pellet was obtained by pressing 30 mg of precursors into a 6 mm-diameter die, under a load of 2 tons. The resulting pellet thickness is approximately 0.5 mm. For a typical TS reaction, a synthesis duration of 20 s was chosen based on preliminary optimization. Extending the synthesis duration from 20 s to 40 s did not improve the superconducting phase fraction; 20 s was therefore selected as the standard TS condition. The solid-state reaction control group was obtained via heating in a muffle furnace (Lindberg Blue M supplied by Thermo Fisher) with a heating rate of 5 K $min^{-1}$, followed by a 12 h isothermal hold at ~1120 K in air (Fig.S4). Conventional synthesis duration and temperature are selected based on commonly used procedures reported in literature without further optimization [4,21].

Sample temperature was monitored during TS using a Raytek MI3-series IR sensor (Fig. 2A). The IR sensor was positioned vertically downward to face the top surface of the W substrate. The temperature profile rises rapidly at ~ 200 K $s^{-1}$ to a plateau near 1100 K, then cools to room temperature at ~ 300 K $s^{-1}$. For comparison, temperature vs. time profile of solid-state reaction (Fig.S4) shows a comparable isothermal temperature ~1120 K, yet the heating and cooling rates are ~$10^4$ times slower than TS. In addition, the reaction duration of 12 h is three orders of magnitude longer. A Keithley 2260B-80–40 programmable direct current (DC) power supply was used as the power source for TS reaction. TS synthesis was run under a current-control condition, with the current set to 40 A, and the voltage varied between 6 and 7 V (Fig. 2B). Spatial temperature non-uniformity during TS is expected across the length of the W substrate due to the large thermal mass of the graphite plates. The highest temperature is reached at the center of the strip, as indicated by localized oxidation in Fig. 1B (ii). Accordingly, TS was performed by positioning the sample at the substrate center to maximize thermal exposure.

$T_c$ was determined by DC and alternating current (AC) susceptibility measurements using a Quantum Design Magnetic Property Measurement System (MPMS-3). The DC magnetization as a function of temperature (Fig. 3A) demonstrates the proof-of-principle that a superconducting phase forms in the Bi–Sr–Ca–Cu–O system under TS within seconds. The onset of diamagnetism occurs approximately at 92 K, indicating the presence of superconductivity. Divergence between zero-field-cooled (ZFC) and field-cooled (FC) curves below $T_c$ is observed, suggesting the presence of flux pinning within the superconducting regions. A minor change in slope is observed within both ZFC and FC measurements (Fig. 3A) at ~ 25 K. A similar low-temperature feature is observed in the precursor mixture (Fig.S5),

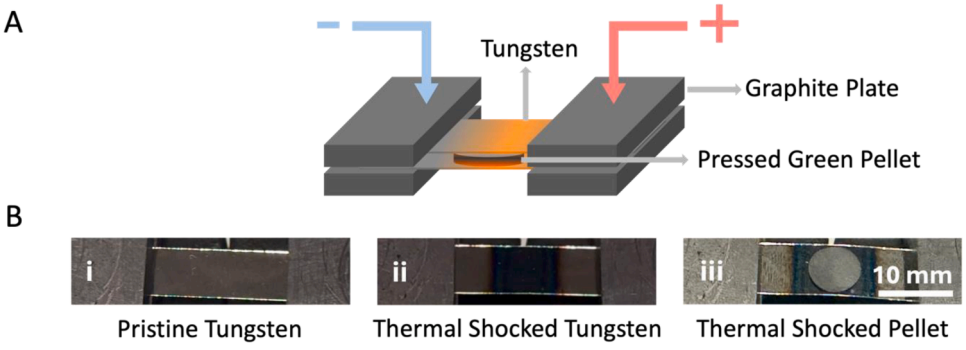


**Fig. 1.** Schematic of thermal shock (TS) setup and tungsten (W) strip evolution throughout TS. A, schematic setup of the TS process. Cold-pressed Bi–Sr–Ca–Cu–O precursor pellet is sandwiched between two W strips. Current passes through the graphite plate to the W strips. Precursor pellet is heated by indirect Joule heating delivered by the W strips. B, i, pristine W strip. ii, TS treated W strip. Five seconds of TS at 40 A allows a formation of $WO_{3-x}$ ($0 \leq x \leq 0.1$) layer. iii, precursor pellet TS treated for 20 s.

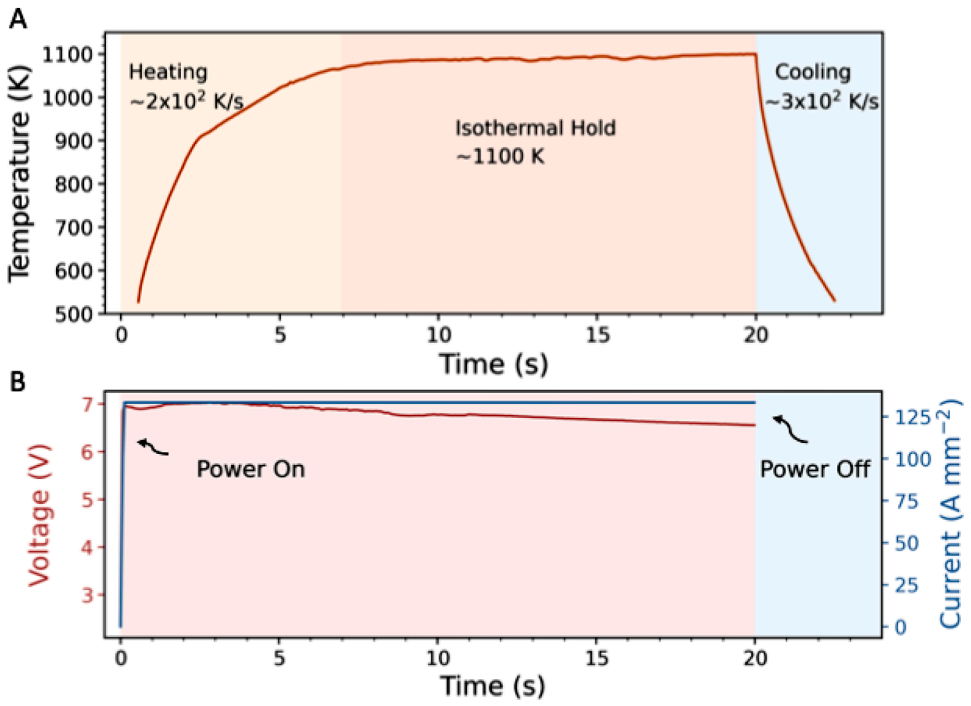


**Fig. 2.** Processing parameters of TS. A, temperature profile of the 20 s TS process. The lower temperature cut-off is limited by the working window of the IR sensor (523 K). B, voltage and current density profiles of TS.

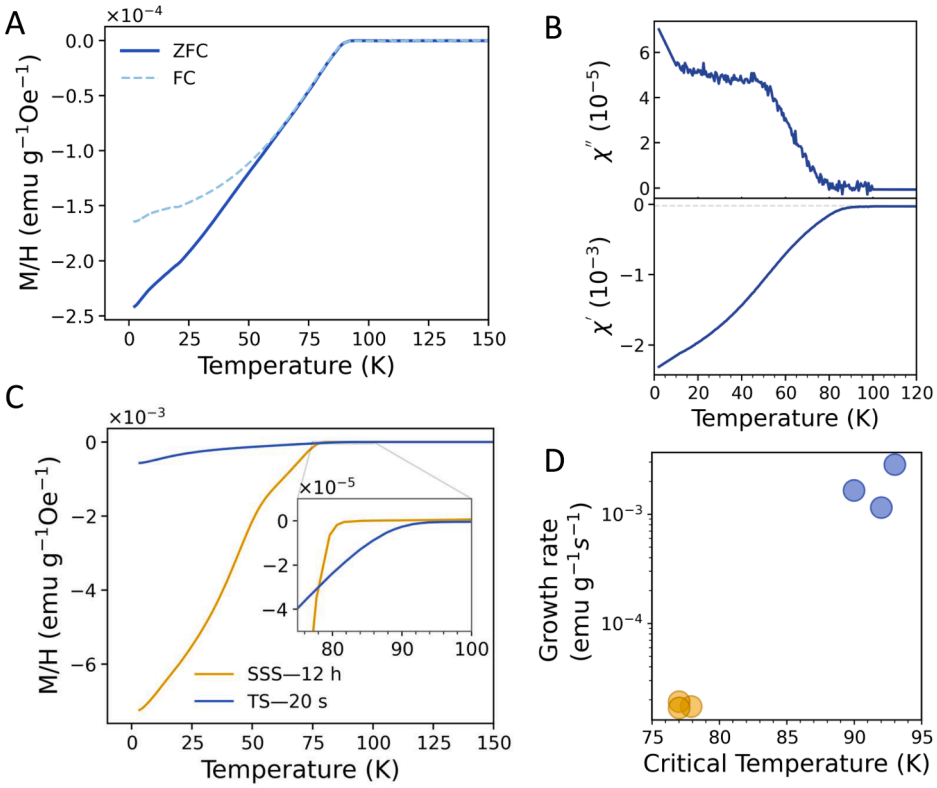


**Fig. 3.** Magnetic measurements of Bi–Sr–Ca–Cu–O. A, zero-field cooled (ZFC) and field cooled (FC) measurement of TS treated Bi–Sr–Ca–Cu–O obtained under an applied magnetic field (*H*) of 100 Oe. *M* denotes magnetic moment in emu $g^{-1}$. Divergence of ZFC and FC starts at 92 K. B, alternating-current (AC) susceptibility measurement of TS treated Bi–Sr–Ca–Cu–O. Measurement was performed with an AC magnetic field amplitude of 5 Oe and frequency of 500 Hz. $\chi'$ and $\chi''$ are in unit emu $g^{-1}$ $Oe^{-1}$. Onset of $\chi'$ peak indicates the emergence of superconductivity at 90–92 K. The lack of $\chi''$ cusp indicates a poorly percolating network. C, direct-current (DC) susceptibility measurement of solid-state sintered for 12 h (SSS–12 hr, in yellow) and thermal shocked for 20 s (TS–20 s, in blue) at 100 Oe. The zoomed-in box shows the superconducting transition of the solid-state sintered sample being 79 K, and the TS sample being 90–92 K. D, superconducting phase growth rate (log scale) vs. critical temperature of SSS–12 hr (in yellow) and TS–20 s (in blue). Three replicate samples were synthesized and measured under each synthesis condition. The measurement was done at 100 Oe.

suggesting that the 25 K transition may arise from precursor-related paramagnetic background. At the same time, DC susceptibility measurement (Fig.S5) also confirms that the precursors themselves exhibit no superconductivity.

AC susceptibility further supports the presence of superconductivity, which can be seen from the negative onset of $\chi'$ starting at 92 K (Fig. 3B). $\chi'$ and $\chi''$ represent the real and imaginary components of AC susceptibility. The broad $\chi'$ transition indicates the presence of inhomogeneous superconducting states. The absence of a pronounced $\chi''$ peak suggests that the superconducting phase is non-percolating and likely consists of isolated superconducting regions embedded in a non-superconducting matrix (Fig. 3B). A similar suppression of the $\chi$" peak has been reported in granular superconductors after grinding solid-state sintered superconducting pellets into fine powders [25]. The broad superconducting transition of the TS–treated sample gives a $T_c$ onset range of 90–92 K, corresponding to the reported $T_c$ of the Bi–2212 phase achieved via traditional solid-state sintering [6].

Fig. 3C shows the DC magnetization as a function of temperature for Bi–Sr–Ca–Cu–O solid-state sintered for 12 h (SSS–12 h) and thermal shocked for 20 s (TS–20 s). Notably, TS–20 s accessed a 15 K higher $T_c$ (90–92 K) than what has been observed in SSS–12 h (~77 K). The baseline comparison to the TS-treated sample is a single-step solid-state synthesized Bi–2212 at 1123 K for 12 h. It is worth noting that the literature $T_c$ for Bi–2212, achieved via solid-state synthesis, is in the range 89–91 K [3]. To achieve Bi–2212 with optimal $T_c$, synthesis requires repetitive grinding and sintering. Here, the solid-state baseline has only been sintered once, as the present comparison intends to isolate the effect of synthesis timescale. Bi–2212 typically also follows sintering at high oxygen partial pressure after air sintering. In the absence of sintering in an oxygen-rich environment, our solid-state sintered value matches the literature result, showing a $T_c$ of ~77 K after 1073 K annealing for 12 h in air [26]. It is known that high-temperature synthesis of the Bi–Sr–Ca–Cu–O compound facilitates high $T_c$ phase formation [4,21]. However, since the TS temperature is slightly below that of solid-state synthesis during their isothermal hold, the higher $T_c$ observed in TS may arise from different kinetic pathways other than pure temperature effect. The rapid heating and cooling offered by TS may suppress undesired phase decomposition and coarsening; it may also kinetically preserve the high-$T_c$ phase formed within Bi–Sr–Ca–Cu–O. Direct oxygen-content measurements of the superconducting phase are needed to determine whether oxygen non-stoichiometry contributes to the observed $T_c$.

It is also observed that the superconducting transition is sharp for SSS–12 h, yet a broader transition is seen in TS–20 s. The broader transition can come from inhomogeneous superconducting phase formation within the TS-treated sample, possibly a result of the short thermal history, fast heating rate, and temperature inhomogeneity within the TS sample pellet. Superconducting shielding fractions of TS–20 s and SSS–12 h, estimated from low-temperature ZFC magnetization, are ~4.7 % and ~59.2 % by weight as compared to the theoretical value of Bi–2212 (calculation shown in SI). The calculated shielding fraction for TS–20 s likely underestimates the true value because of its non-percolating nature as shown in Fig. 3B. The limited superconducting phase fraction in TS–20 s may result from the short synthesis duration of 20 s, and the ease of $Bi_2Sr_2CuO_{6+y}$ (commonly referred to as Bi–2201) phase formation at a lower synthesis temperature [5].

Fig. 3D shows the superconducting phase growth rate (logarithmic scale) and $T_c$ for triplicate syntheses under solid-state sintering and TS conditions. Superconducting phase growth rate is defined as the shielding fraction divided by the total synthesis time. TS synthesizes the superconducting phase ~100 × faster than solid-state sintering, though with lower reproducibility across replicates. This variability across TS–20s samples likely reflects the sensitivity of ultrafast processing to precursor mixing. While the superconducting phase fraction in TS remains limited, the rapid emergence of a high $T_c$ phase within seconds highlights the potential of thermal shock as a fast-screening tool. Further optimization, including achieving nano-scale homogeneous precursor mixing, fine-tuning synthesis parameters, and optimizing substrate durability and chemical stability, is needed to amplify the superconducting phase fraction and reproducibility.

Fig. 4A and B show scanning electron microscopy (SEM) images of SSS–12 h and TS–20 s samples, respectively. SEM images reveal distinct microstructural features of SSS–12 h and TS–20 s arising from their different thermal histories. SSS–12 h sample (Fig. 4A) exhibits plate-like grains and platelet aggregates, indicating substantial grain growth occurred during the prolonged solid-state sintering. In contrast, the TS–20 s sample (Fig. 4B) shows a more porous and irregular morphology, with smaller and less-developed platelet structures. The observed morphology in TS is consistent with its short thermal exposure; short duration of TS enables rapid phase formation yet restricts long-range diffusion and grain growth. The increase in porosity and reduction in grain size in TS–20 s sample may contribute to the broader and weaker magnetic response [27,28], in addition to the presence of differences in superconducting phase fraction and phase purity.

X-ray diffraction (XRD) pattern matching supports the formation of Bi–Sr–Ca–Cu–O phases after TS and SSS treatment (Fig. 5). The precursor mixture shows peaks from the starting oxides, with only $Bi_2O_3$ peaks marked for simplicity (Fig. 5A). The SSS–12 h sample shows reflections consistent with Bi–2212 and Bi–2201 (Fig. 5B). The TS–20 s sample also shows Bi–2212 and Bi–2201 reflections, together with residual precursor and possible intermediate phases, indicating incomplete reaction during the short thermal exposure (Fig. 5C). The weak Bi–2212-like phase reflections in TS–20 s are consistent with the limited superconducting phase fraction inferred from magnetic measurements. Because Bi–2212 and Bi–2201 peaks strongly overlap, XRD only provides qualitative support of Bi–2212-like phase formation.

To assess the generality of the TS approach for oxide superconductor synthesis, we applied identical TS procedures to Y–Ba–Cu–O precursors (precursor chemistry and stoichiometry shown in SI), where superconductivity with a $T_c$ of ~93 K was observed from DC susceptibility (Fig. S6).

In summary, we demonstrate the formation of a superconducting phase in the Bi–Sr–Ca–Cu–O system by TS within seconds, approximately 100 × faster than single-step solid-state sintering. The approach circumvents the fundamental incompatibility between carbon-based ultrafast synthesis techniques and oxygen-requiring cuprate synthesis. Although the superconducting phase fraction remains limited in this proof-of-principle demonstration, the observed $T_c$ of 90–92 K within Bi–Sr–Ca–Cu–O demonstrates that ultrafast processing can synthesize and preserve superconducting phases. Extension to Y–Ba–Cu–O moves the existing approach beyond specific systems. These results establish TS as a high-throughput synthesis platform for exploring both synthesis conditions and novel chemistries in oxide superconductors. TS also potentially offers a new route to achieve metastable superconducting phases that are otherwise kinetically inaccessible and time-consuming by conventional solid-state synthesis. Direct field-assisted methods such as flash sintering should also be considered in future work, as they may offer a complementary route to explore and distinguish the thermal, electrical, and electrochemical contributions to ultrafast superconducting phase formation [29].

## CRediT authorship contribution statement

**Vivienne Yiwei Liu:** Writing – review & editing, Writing – original draft, Visualization, Validation, Methodology, Investigation, Formal analysis. **Weiyin Chen:** Writing – review & editing, Validation, Methodology, Investigation. **Yimeng Huang:** Writing – review & editing, Validation, Methodology, Investigation. **Zihan Lin:** Writing – review & editing, Methodology, Investigation, Formal analysis. **Ethan Yupeng Zheng:** Writing – review & editing, Investigation. **Yaoshen Niu:** Writing – review & editing, Investigation, Formal analysis. **Bowen Zhang:**

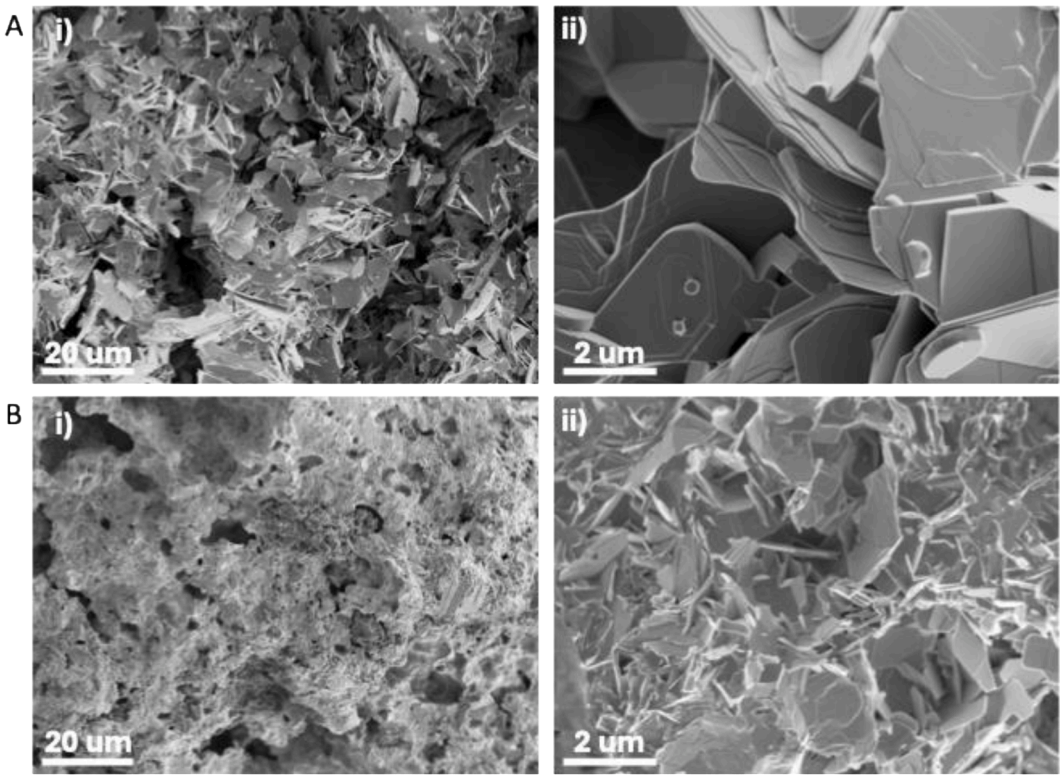


**Fig. 4.** Scanning electron microscopy (SEM) images of Bi–Sr–Ca–Cu–O. A, solid-state sintered sample prepared at 1123 K for 12 h (SSS–12 h), showing plate-like grains and platelet aggregates under both low (i) and high (ii) magnifications. B, thermal shocked sample for 20 s (TS–20 s) showing a porous morphology under low magnification in (i) and smaller, less developed platelet-like features under high magnification in (ii).

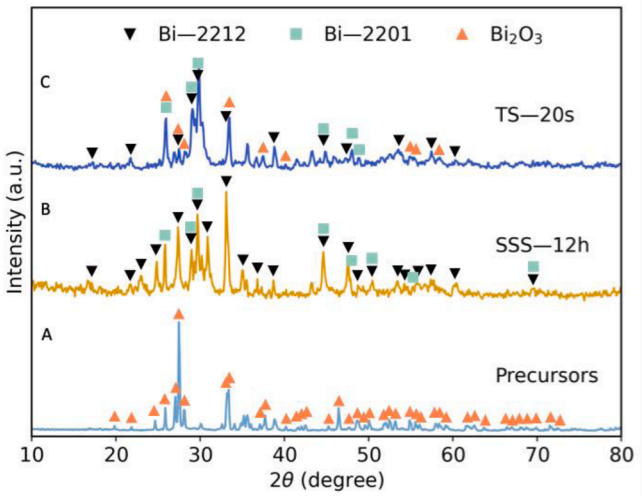


**Fig. 5.** X-ray diffraction (XRD) pattern of Bi–Sr–Ca–Cu–O. XRD result is obtained using Cu $K_\alpha$ Malvern Panalytical X'Pert Pro. Reference peak positions for Bi–2212 (PDF# 00–040–0277), Bi–2201 (PDF# 04–017–7328), and $Bi_2O_3$ (PDF# 04–011–1986) are shown for comparison. Only $Bi_2O_3$ is included as a representative precursor phase for simplicity. A, precursor mixture consisting of $Bi_2O_3$, SrO, CaO, and CuO. B, solid-state sintered sample at 1123 K for 12 h (SSS–12 h), showing peaks consistent with Bi–2212 and Bi–2201. C, thermal shocked sample for 20 s (TS–20), showing peaks consistent with Bi–2212, Bi–2201, and unreacted precursors.

Writing – review & editing, Methodology. **Ju Li:** Writing – review & editing, Supervision, Resources, Project administration, Funding acquisition, Conceptualization.

## Declaration of competing interest

The authors declare that they have no known competing financial interests or personal relationships that could have appeared to influence the work reported in this paper.

## Acknowledgements

We acknowledge support by the MIT-Google Program for Computing Innovation, as well as Gordon and Betty Moore Foundation's EPiQS Initiative, Grant GBMF11945. We thank Dr. Rafael Jaramillo for scientific discussions and funding acquisition. This work was carried out in part using MIT.nano facilities.

## Supplementary materials

Supplementary material associated with this article can be found, in the online version, at doi:10.1016/j.scriptamat.2026.117482.

## References

[1] M.R. Beasley, T.H. Geballe, Superconducting materials, Phys. Today 37 (1984) 60–68, https://doi.org/10.1063/1.2915921.
[2] N. Chen, S.J. Rothman, J.L. Routbort, Diffusion of Sr in $Bi_2Sr_2Ca_{n-1}Cu_nO_{2n+4}$, J. Mater. Res. 8 (1993) 2465–2470, https://doi.org/10.1557/JMR.1993.2465.
[3] H. Eisaki, N. Kaneko, D.L. Feng, A. Damascelli, P.K. Mang, K.M. Shen, Z.-X. Shen, M. Greven, Effect of chemical inhomogeneity in bismuth-based copper oxide superconductors, Phys. Rev. B 69 (2004) 064512, https://doi.org/10.1103/PhysRevB.69.064512.
[4] S.M. Khalil, A. Sedky, Annealing temperature effect on the properties of Bi:2212 superconducting system, Phys. B: Condens. Matter 357 (2005) 299–304, https://doi.org/10.1016/j.physb.2004.11.080.
[5] L.M. Rubin, T.P. Orlando, J.B. Vander Sande, G. Gorman, R. Savoy, R. Swope, R. Beyers, Phase stability limits and solid-state decomposition of $Bi_2Sr_2CaCu_2O_{8+\delta}$ and $Bi_2Sr_2Ca_2Cu_3O_{10+\delta}$ in reduced oxygen pressures, Phys. C: Supercond. 217 (1993) 227–234, https://doi.org/10.1016/0921-4534(93)90817-A.

[6] M.A. Subramanian, C.C. Torardi, J.C. Calabrese, J. Gopalakrishnan, K.J. Morrissey, T.R. Askew, R.B. Flippen, U. Chowdhry, A.W. Sleight, A new high-temperature superconductor: $Bi_2Sr_{3-x}Ca_xCu_2O_{8+y}$, Science 239 (1988) 1015–1017, https://doi.org/10.1126/science.239.4843.1015.
[7] S.L.E. Chow, Z. Luo, A. Ariando, Bulk superconductivity near 40 K in hole-doped $SmNiO_2$ at ambient pressure, Nature 642 (2025) 58–63, https://doi.org/10.1038/s41586-025-08893-4.
[8] D. Li, K. Lee, B.Y. Wang, M. Osada, S. Crossley, H.R. Lee, Y. Cui, Y. Hikita, H. Y. Hwang, Superconductivity in an infinite-layer nickelate, Nature 572 (2019) 624–627, https://doi.org/10.1038/s41586-019-1496-5.
[9] G. Zhou, W. Lv, H. Wang, Z. Nie, Y. Chen, Y. Li, H. Huang, W.-Q. Chen, Y.-J. Sun, Q.-K. Xue, Z. Chen, Ambient-pressure superconductivity onset above 40 K in $(La, Pr)_3Ni_2O_7$ films, Nature 640 (2025) 641–646, https://doi.org/10.1038/s41586-025-08755-z.
[10] E.L. Brosha, P.K. Davies, F.H. Garzon, I.D. Raistrick, Metastability of superconducting compounds in the Y-Ba-Cu-O system, Science 260 (1993) 196–198, https://doi.org/10.1126/science.260.5105.196.
[11] J.D. Jorgensen, Defects and superconductivity in the copper oxides, Phys. Today 44 (1991) 34–40, https://doi.org/10.1063/1.881304.
[12] J.D. Jorgensen, D.G. Hinks, P.G. Radaelli, S. Pei, P. Lightfoot, B. Dabrowski, C. U. Segre, B.A. Hunter, Defects, defect ordering, structural coherence and superconductivity in the 123 copper oxides, Phys. C: Supercond. 185-189 (1991) 184–189, https://doi.org/10.1016/0921-4534(91)91970-F, 185–189.
[13] J.C. Phillips, Lattice instabilities and high-temperature superconductivity, Phys. Rev. Lett. 26 (1971) 543–546, https://doi.org/10.1103/PhysRevLett.26.543.
[14] A.W. Sleight, Synthesis of oxide superconductors, Phys. Today 44 (1991) 24–30, https://doi.org/10.1063/1.881303.
[15] Y. Yao, Z. Huang, P. Xie, S.D. Lacey, R.J. Jacob, H. Xie, F. Chen, A. Nie, T. Pu, M. Rehwoldt, D. Yu, M.R. Zachariah, C. Wang, R. Shahbazian-Yassar, J. Li, L. Hu, Carbothermal shock synthesis of high-entropy-alloy nanoparticles, Science 359 (2018) 1489–1494, https://doi.org/10.1126/science.aan5412.
[16] C. Wang, W. Ping, Q. Bai, H. Cui, R. Hensleigh, R. Wang, A.H. Brozena, Z. Xu, J. Dai, Y. Pei, C. Zheng, G. Pastel, J. Gao, X. Wang, H. Wang, J.-C. Zhao, B. Yang, X. Zheng, J. (Rayne) Luo, Y. Mo, B. Dunn, L. Hu, A general method to synthesize and sinter bulk ceramics in seconds, Science 368 (2020) 521–526, https://doi.org/10.1126/science.aaz7681.
[17] D.X. Luong, K.V. Bets, W.A. Algozeeb, M.G. Stanford, C. Kittrell, W. Chen, R. V. Salvatierra, M. Ren, E.A. McHugh, P.A. Advincula, Z. Wang, M. Bhatt, H. Guo, V. Mancevski, R. Shahsavari, B.I. Yakobson, J.M. Tour, Gram-scale bottom-up flash graphene synthesis, Nature 577 (2020) 647–651, https://doi.org/10.1038/s41586-020-1938-0.
[18] Z. Zhang, Z. Ren, C.-W. Hsu, W. Chen, Z.-W. Hong, C.-F. Lee, A. Penn, H. Xu, D. J. Zheng, S. Miao, Y. Huang, Y. Gao, W. Chen, H. Smith, Y. Niu, Y. Tian, Y.-R. Lu, Y.-C. Shao, S. Li, H.-T. Wang, I.I. Abate, P. Agrawal, Y. Shao-Horn, J. Li, A multimodal robotic platform for multi-element electrocatalyst discovery, Nature 647 (2025) 390–396, https://doi.org/10.1038/s41586-025-09640-5.
[19] S.-W. Park, H. Kim, S. Han, K.S. Kim, Y.-Y. Song, H.-G. Lee, W. Jang, D.-H. Lee, S. Bae, D. Kim, J. Park, I. Park, S.-C. Nam, H. Kim, J. Lee, K. Kang, D.-H. Seo, High-throughput synthesis of Mn-based disordered rock-salt Li-ion cathodes with improved rate capability via rapid joule-heating, Adv. Energy Mater. 15 (2025) e03496, https://doi.org/10.1002/aenm.202503496.
[20] W. Fan, Z. Ren, Z. Sun, X. Yao, B. Yildiz, J. Li, Synthesizing functional ceramic powders for solid oxide cells in minutes through thermal shock, ACS Energy Lett. 7 (2022) 1223–1229, https://doi.org/10.1021/acsenergylett.1c02630.
[21] H. Maeda, Y. Tanaka, M. Fukutomi, T. Asano, A new high-Tc oxide superconductor without a rare Earth element, Jpn. J. Appl. Phys. 27 (1988) L209, https://doi.org/10.1143/JJAP.27.L209.
[22] T. Wada, N. Suzuki, A. Maeda, T. Yabe, K. Uchinokura, S. Uchida, S. Tanaka, Preparation and properties of superconducting $La_{1+x}Ba_{2-x}Cu_3O_y$ ($0 \leq x \leq 0.5$) ceramics sintered in $N_2$ gas atmosphere, Phys. Rev. B 39 (1989) 9126–9138, https://doi.org/10.1103/PhysRevB.39.9126.
[23] R. Li, G. Álvarez, A. Ipakchi, L. Cupertino-Malheiros, M.R. Gilbert, E. Martínez-Pañeda, E. Prestat, Understanding the oxidation of pure tungsten in air and its impact on the lifecycle of a fusion power plant, Nucl. Mater. Energy 45 (2025) 101988, https://doi.org/10.1016/j.nme.2025.101988.
[24] W.W. Webb, J.T. Norton, C. Wagner, Oxidation of tungsten, J. Electrochem. Soc. 103 (1956) 107, https://doi.org/10.1149/1.2430238.
[25] D.-X. Chen, R.B. Goldfarb, J. Nogués, K.V. Rao, Magnetic susceptibility of sintered and powdered Y-Ba-Cu-O, J. Appl. Phys. 63 (1988) 980–983, https://doi.org/10.1063/1.340050.
[26] R.H. Patel, A. Nabialek, M. Niewczas, Characterization of superconducting properties of BSCCO powder prepared by attrition milling, Supercond. Sci. Technol. 18 (2005) 317–324, https://doi.org/10.1088/0953-2048/18/3/019.
[27] F. Kahraman, A. Sotelo, M.A. Madre, J.C. Diez, B. Ozkurt, Sh. Rasekh, Relationship between microstructure and superconducting properties in hot-pressed Bi-2212/Ag ceramic composites, Ceram. Int. 41 (2015) 14924–14929, https://doi.org/10.1016/j.ceramint.2015.08.029.
[28] J. Kumar, D. Sharma, P.K. Ahluwalia, V.P.S. Awana, Enhanced superconducting performance of melt quenched Bi2Sr2CaCu2O8 (Bi-2212) superconductor, Mater. Chem. Phys. 139 (2013) 681–688, https://doi.org/10.1016/j.matchemphys.2013.02.016.
[29] R. Raj, A. Kulkarni, J.-M. Lebrun, S. Jha, Flash sintering: a new frontier in defect physics and materials science, MRS Bulletin 46 (2021) 36–43, https://doi.org/10.1557/s43577-020-00011-1.
[30] A.W. Sleight, Crystal chemistry of oxide superconductors, Phys. C: Supercond. Appl. 162-164 (1989) 3–7, https://doi.org/10.1016/0921-4534(89)90894-0, 162–164.